Engineering Fracture Mechanics 210 (2019) 3–12

Contents lists available at ScienceDirect

Engineering Fracture Mechanics

journal homepage: www.elsevier.com/locate/engfracmech

Influence of snap-back instabilities on Acoustic Emission damage monitoring

Giuseppe Lacidogna, Federico Accornero*, Alberto Carpinteri

Department of Structural, Geotechnical and Building Engineering, Politecnico di Torino, Italy

ARTICLE INFO

Keywords:
Snap-back instability
Brittleness
Damage monitoring
Acoustic Emission
Crushing and fracture energy

ABSTRACT

Experimental tests are carried out to evidence the energy emitted during snap-back instabilities of rock specimens in compression. Several gypsum samples with different slenderness are considered, and all the tests are monitored by means of the Acoustic Emission (AE) technique. In particular, the cumulated number of AE signals is used to represent the emitted energy. The performed tests have been controlled in compression in two different ways: through vertical or circumferential displacement, by imposing in both cases a constant displacement rate.

For the tests controlled by the vertical displacement, in the more brittle cases crack propagation suddenly occurs with a catastrophic drop in the load carrying capacity, and the resulting emitted energy appears with a burst in the AE cumulated curve. When the tests are controlled by the circumferential elongation, the damage increment is measured with a roller-link chain wrapped around the cylindrical samples at mid-height in order to obtain the complete load vs. displacement response. In the brittle cases, both load and vertical displacement decrease to obtain a controlled crack propagation: the energy is totally dissipated and consequently no emissions due to snap-back phenomena are observed, proving that crushing or fracture energy and AE energy are independent physical quantities, the latter resulting from local instabilities in the structural response.

1. Introduction

The compressive failure of brittle materials such as rocks and concrete is mainly characterized by the nucleation, growth, and coalescence of microcracks and defects, involving wide ranges of time and length scales [1–3]. According to experimental evidences, the post-peak phase of the loading process is characterized by a strong strain localization, independently of the actual collapse mechanism of the structural element. Consequently, in the softening regime, energy dissipation takes place over an internal surface rather than within the whole specimen volume, in close analogy with the behavior in tension [4].

The shape of the structural load-displacement curve changes substantially by varying the size-scale with the structure geometry remaining unchanged [1,2,5]. The softening branch becomes steeper when the size-scale increases. For size-scales larger than the critical one (regarding an infinite softening slope), the post-peak branch presents a positive slope and part of the load-displacement path becomes virtual if the loading process is displacement-controlled. In extremely brittle cases, crack propagation occurs suddenly with a catastrophic drop in the load carrying capacity. This means that both load and displacement must decrease to obtain a controlled crack propagation [6]. Such a phenomenon, the so-called snap-back instability, was deeply investigated with reference to the crack growth analysis in elastic-softening materials [6–8]. In the framework of Linear Elastic Fracture Mechanics, it reproduces

* Corresponding author.
E-mail address: federico.accornero@polito.it (F. Accornero).

https://doi.org/10.1016/j.engfracmech.2018.06.042
Received 22 February 2018; Received in revised form 26 June 2018; Accepted 27 June 2018
Available online 28 June 2018
0013-7944/

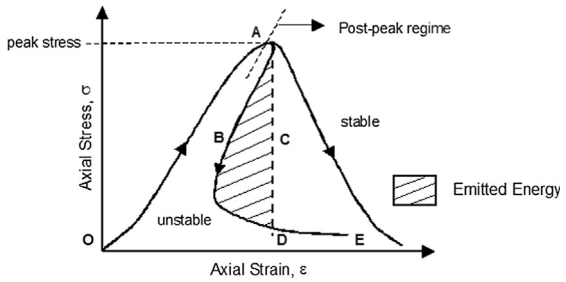

Fig. 1. Stable and catastrophic (snap-back) response. The emitted energy during snap-back instability is highlighted by the dashed area.

the classical Griffith instability for very brittle systems, depending on structural geometry and material properties [6].

The size-scale transition from ductile to brittle behavior is governed by a non-dimensional brittleness number, s_E, which is a function of material properties and structure size-scale [9]. A truly brittle failure occurs only with relatively low fracture energies G_{IC}, high tensile strengths σ_u, and/or large structure size-scales b, i.e. when $s_E = G_{IC}/\sigma_u b \rightarrow 0$. On the other hand, if the loading process is controlled by a monotonically increasing function of time, i.e., like the crack mouth opening displacement, the snap-back instability can be experimentally captured.

2. Dissipated and emitted energy

Some information on the modalities of energy release and the development of cracking patterns can be obtained on the basis of the Acoustic Emission (AE) monitoring technique, that proves possible to detect the occurrence and evolution of stress-induced cracks [10–15]. As a matter of fact, cracking comes along with the emission of elastic waves which propagate inside the material. These waves can be detected by transducers applied to the surface of structural elements. The AE technique was at first used to identify defects, cracks and plastic deformations in metallic materials, and only then has been extended to studies in the field of quasi-brittle materials like rocks and concrete, where it can be used for the diagnosis of structural damage phenomena [16–23].

Recently, it has been shown that the energy emission is proportional to the cumulative number of AE events and it is a surface-dominated phenomenon. This has been demonstrated by interpreting AE data with statistical and fractal concepts [4]. Analogously, also the localization of microcracks distribution within the specimen volume by means of the AE technique has physically confirmed the localization of the energy emission over preferential bands and surfaces during the damage evolution [24].

Moreover, according to very recent interpretations [6,25], the relationship between crack propagation and emitted energy, if analyzed by Acoustic Emissions (AE), is represented by the area subtended by each snap-back branch (Fig. 2). In fact, in a loading

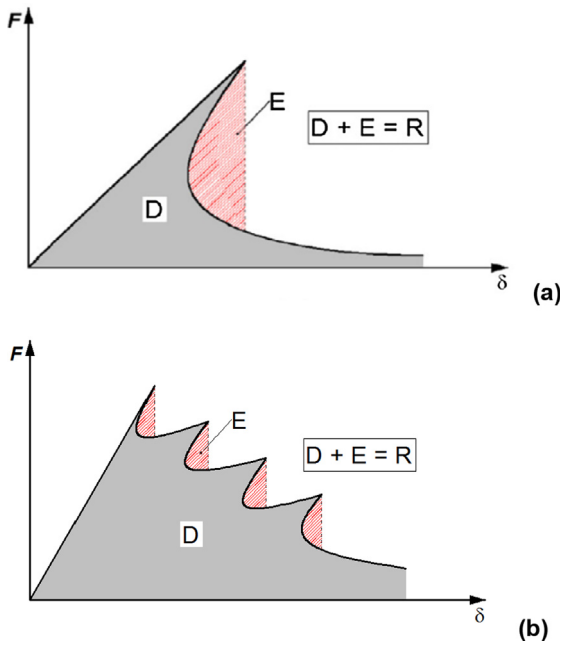

Fig. 2. Load-displacement curves representing: (a) a catastrophic behavior (single snap-back); (b) a global softening behavior perturbed by multiple local instabilities (snap-back). The grey areas identify the dissipated energy, D, whereas the pink ones represent the emitted energy, E. The total released energy, R, is the summation of the two previous ones: D + E = R [6,25].

process, the total energy released during the test, R, is equal to the sum of the dissipated energy, D (grey area in Fig. 2), plus the emitted energy during the snap-back phenomena, E (pink area in Fig. 2).

In the present paper, the emitted energy is experimentally detected during snap-back instabilities of gypsum specimens in compression. This energy is derived on the basis of the AE monitoring performed during the tests. In particular, to compute the emitted energy the cumulated number of AE signals is employed. For the more brittle cases, crack propagation suddenly occurs with a catastrophic drop in the load carrying capacity, therefore the consequent emitted energy appears with a burst in the cumulated AE curve. On the other hand, in order to obtain the complete load vs. displacement response, some tests are controlled, during the damage increase, by a linked chain placed around the cylinder at mid-height. In the brittle cases, both load and displacement must decrease to obtain a controlled crack propagation, and consequently no emitted energy is observed.

3. Mechanical instabilities and emitted energy: Global or local snap-back phenomena

The mechanical behavior of a specimen subjected to uniaxial compression can be described by three different stages [3,13,26]. A first stage that takes into account the initiation and propagation of microcracks. By approaching the compressive strength, such microcracks coalesce forming macrocracks, and localizing over a preferential surface. In the second stage, the ultimate compressive strength, σ_u, is reached, and the inelastic deformations are localized in a crushing band. The behavior of this zone is described by a softening law according to [26], whereas the remaining part of the specimen still behaves elastically. Finally, in the third stage, the material in the crushing zone is completely damaged. Very different global responses in the stress-strain diagram can be obtained by varying the mechanical and geometrical parameters of the sample [13]. In particular, the softening process is stable under displacement control only when the slope in the softening regime is negative (Fig. 1). A sudden drop in the load bearing capacity under displacement control takes place when the slope is infinite. Finally, the snap-back instability is avoided if the loading process is controlled by means of the circumferential elongation, the slope of the softening branch being positive. Analogously to quasi-brittle materials subjected to tension, the stability of the overall behavior of specimens in compression depends on geometrical (size and slenderness) and mechanical (crushing energy and compression strength) parameters [3]. In accordance with previous studies [26], a catastrophic softening (snap-back) occurs when the global brittleness, B, is:

$$B = \frac{S_{E,c}}{\varepsilon_c \lambda} \leqslant \frac{1}{2.3} \tag{1}$$

where $\lambda = l/b$ is the specimen slenderness, ε_c is the critical compression strain, and $s_{E,c}$ is the energy brittleness number in compression [26]. Therefore, the stability of the compression process is governed by Eq. (1).

In this paper, an experimental correlation is found between the emitted energy, E, and global or local snap-back instabilities of gypsum specimens in compression.

4. Testing on gypsum samples controlled by vertical displacement

In this section, the results of compression tests carried out on three gypsum specimens having diameter equal to 80 mm, and slenderness equal to 2.0, 1.0, and 0.5 are presented (Fig. 3). As recently stated [27], gypsum rocks subjected to compression tests display characteristic fracture phenomena, associated to remarkable crack patterns and coalescence at macroscopic and microscopic scales in the post-peak regime. As a matter of fact, brittle materials such as naturally occurring rocks like granite or serpentinite contain pre-existing micro-cracks, which control the failure mechanism and determine the structural strength. The propagation and coalescence of cracks initiating from such pre-existing defects, on a variety of scales, are the dominant failure mechanisms governing

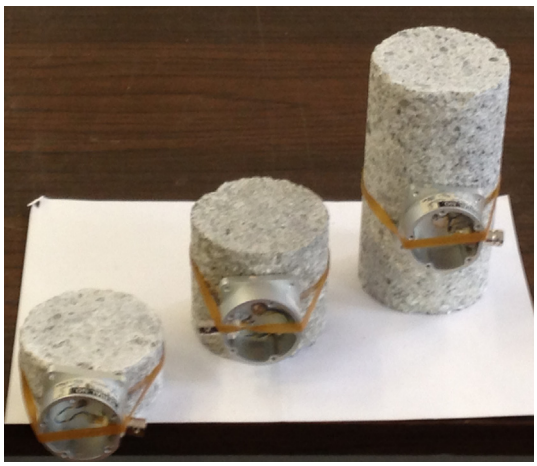

Fig. 3. Compression tests: gypsum specimens.

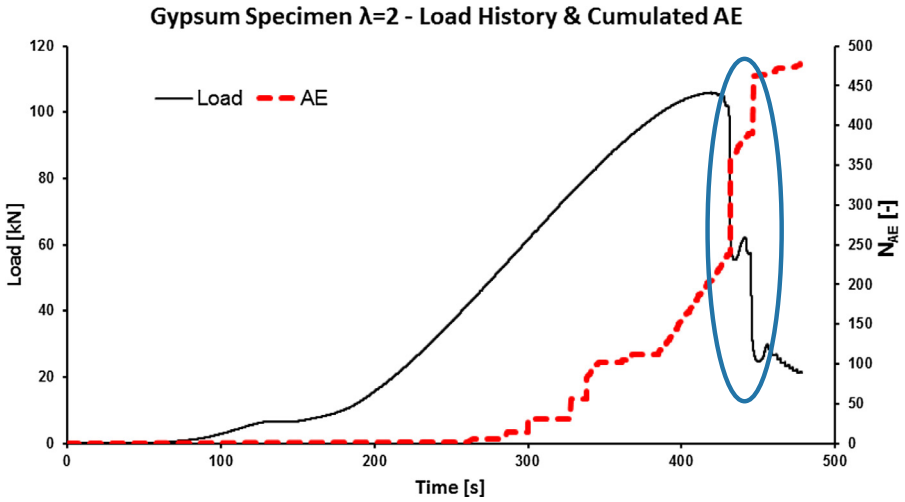

Fig. 4. Load vs time diagram and AE cumulated curve for a gypsum specimen of slenderness 2 subjected to a compression test. An evident correlation emerges between the loading drops (snap-back instabilities) in the post-peak regime, and the AE bursts (emitted energy, E) in the cumulated curve.

the strength and integrity of brittle materials [28–31]. Moreover, AE technique has been effectively employed in the study of fracture phenomena, damage mechanisms, and related fault growth in rocks [32–34].

During experimental tests, the loading process has been controlled by the axial displacement and imposing a constant displacement rate to the upper loading platen, equal to 0.005 mm/s for all specimens, in order to detect all snap-back instabilities. Such a control has permitted to detect the catastrophic drops in the load carrying capacity, both global and local. This catastrophic behavior hides a positive slope in the post-peak softening branch, but, at the same time, it allows the emitted energy to be detected.

During the tests, the specimens were equipped with a thin layer of Teflon in contact between the platen of the testing machine and the specimen ends, to avoid the friction on the bases and facilitate the transversal deformation. Each specimen is monitored by the AE technique. The AE signals (hits) emerging from the compressed specimens were detected by applying to the sample surface a piezoelectric (PZT) transducer, sensitive in the frequency range from 50 to 800 kHz for detection of high-frequency AEs [35]. The sensor is glued with silicone resin on the specimen surface.

The load vs. time diagrams for the three considered cylindrical specimens are shown in Figs. 4 and 6, together with the AE cumulated curves. According to the expectations, the more slender specimen has exhibited a more brittle behavior with a global snap-

Fig. 5. Final collapse for gypsum specimen of slenderness 2: Dominant sub-vertical crack.

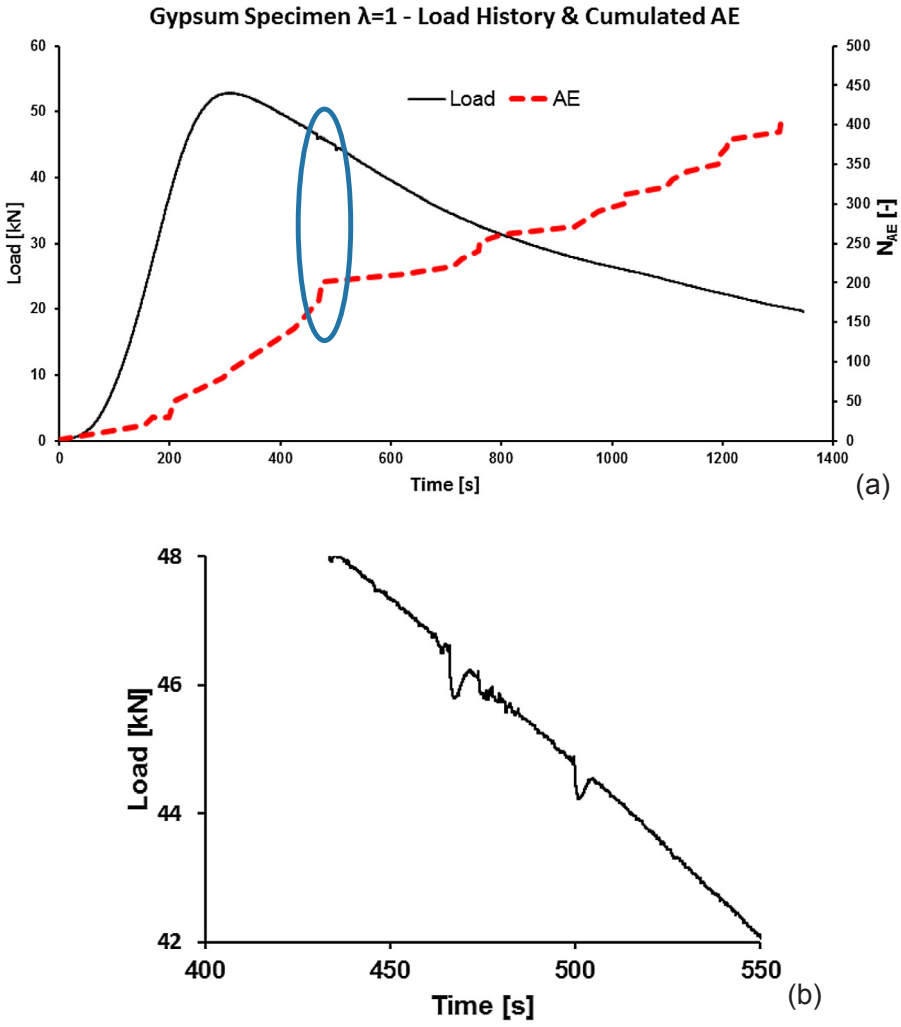

Fig. 6. Load vs time diagram and AE cumulated curve (a) for a gypsum specimen of slenderness 1 subjected to a compression test. A correlation emerges between the slight and multiple loading drops (local snap-back instabilities) (b), and the slight and multiple AE jumps (emitted energy, E) in the cumulated curve.

back instability, the post-peak branch being almost vertical compared to that of the other specimens, characterized by a softening response.

As regards the AE monitoring, the signals were detected by piezoelectric dedicated sensors. The sampling frequency of recording waveforms was set to 1 Msample/s. The data were collected by a National Instruments digitizer capable up to 8 channels AE sensors. The AE waves captured by the sensors were amplified with 60 dB gain before being processed, setting the acquisition threshold level up to 2 mV.

As regards the gypsum specimen with slenderness $\lambda = 2.0$, two severe global snap-back instabilities were detected in the post-peak branch of the load vs time diagram (Fig. 4). Moreover, an evident correlation emerges between the catastrophic drops (snap-back instabilities) in the post-peak regime of the loading process and the AE bursts (emitted energy, E) in the cumulated curve. Due to the slenderness of the specimens, the failure mode observed during the experiment is governed by a dominant sub-vertical crack, leading the damage evolution up to the final collapse (Fig. 5).

The load vs. time diagram of the gypsum specimen with slenderness $\lambda = 1.0$ is shown in Fig. 6a. As previously remarked, whereas the more slender specimen has exhibited a global snap-back instability, the post-peak branch being almost vertical, the specimen with $\lambda = 1.0$ is characterized by a typical softening response. Nevertheless, the softening post-peak regime is perturbed by slight local snap-back instabilities (Fig. 6b), generating multiple and almost continuous AE jumps in the cumulated curve (Fig. 6a). It is worth noting the link between a globally smooth softening branch, and the corresponding AE cumulated curve: the smaller the snap-back instabilities in the loading process, the smoother the AE cumulated curve.

The load vs. time diagram of the gypsum specimen with slenderness $\lambda = 0.5$ is shown in Fig. 7. It is characterized by a ductile response in the post-peak stage of the loading process. A global snap-back instability was detected just after the peak load, at the same

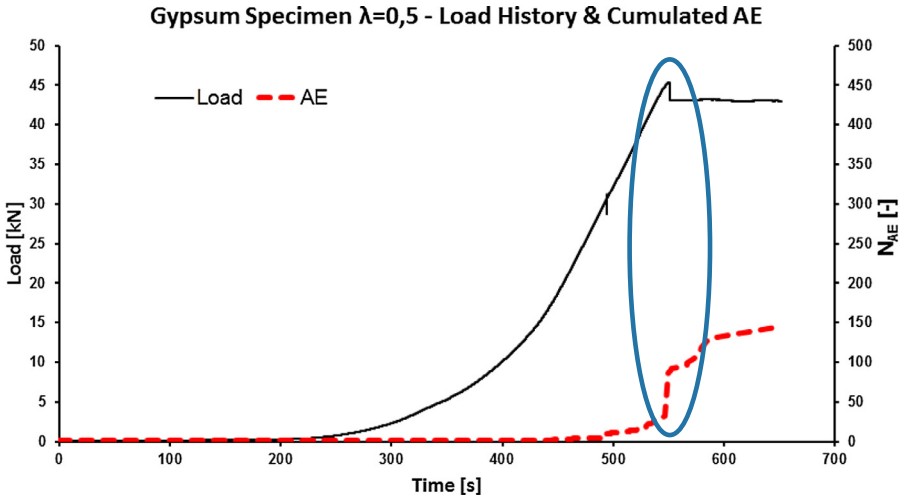

Fig. 7. Load vs time diagram and AE cumulated curve for a gypsum specimen of slenderness 0.5 subjected to a compression test. An evident correlation emerges between the loading drops (snap-back instabilities) in the post-peak regime and the AE bursts (emitted energy, E) in the cumulated curve.

time as an evident AE burst (emitted energy, E) in the cumulated curve (Fig. 7).

5. Fractal domain of the emitted energy

From the fragmentation theory point of view, it can be shown that the energy detected during microcrack propagation, E, is emitted over a fractal domain comprised between a surface and a volume [4,11,36]. As a result, the following size-scaling law has been assumed for the energy emission during fragmentation:

$$E \propto V^{(3-d)/3}, \tag{2}$$

where the fractal exponent, $(3 - d)$, is comprised between 2.0 and 3.0 [4], while the parameter d represents the dimensional decrement with respect to 3. Considering L as the characteristic dimension of the specimen, we have $V^{(3-d)/3} = V^{(1-d/3)} = V/V^{d/3} = L^3/L^d$. If $d = 0.0$, damage will be distributed in the whole specimen volume, i.e., $L^3/1 = L^3$. On the contrary, if d is approaching to 1.0, damage will be organized on a preferential surface, i.e., $L^3/L = L^2$.

This implies that not the true energy density but a fractal energy density (having non-integer physical dimensions)

$$\Gamma = \frac{E}{V^{(3-d)/3}}, \tag{3}$$

can be considered as the size-independent parameter.

On the other hand, during microcrack propagation, AE can be clearly detected. The energy emission, E, is proportional to the number N_{max} of AE signals. Accordingly to the energy emission from a fractal domain, the number of AE signals, N_{max}, not over a volume but over a fractal domain, can be considered as the size-independent parameter:

$$\Gamma_{\mathrm{AE}} = \frac{N_{\max}}{V^{(3-d)/3}}, \tag{4}$$

where Γ_{AE} is the value of AE signals fractal density [11].

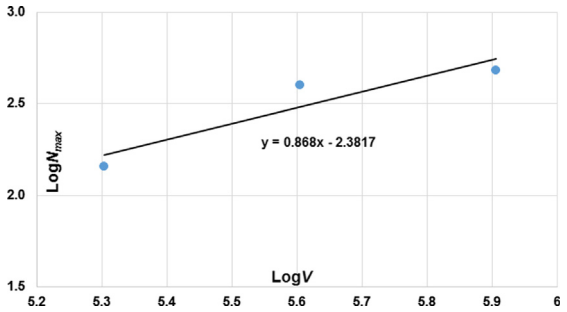

Fig. 8. AE size-scaling in damage evolution.

Fig. 9. Compression tests on a gypsum specimen controlled by the circumferential elongation.

The size-scaling on N_{max} is represented as a function of the specimen volume, fitted to the experimental data (Fig. 8). A slope in the log-log plane close to 0.87 emphasizes that the energy emission occurs in a fractal domain comprised between a volume and a surface. Thus, the fractal AE energy density is about $2\,cm^{-2.61}$ (mean value).

6. Loading processes controlled by circumferential elongation

In this section, the results of compression tests carried out on two gypsum cylindrical specimens having diameter equal to 80 mm, and slenderness equal to 2.0 and 1.0 are presented. The loading process has been controlled by the circumferential elongation, measured by means of an extensometer attached to the ends of a linked chain with roller at each hinge, and placed around the cylinder at mid-height (Fig. 9). Such a damage control, obtained by imposing a constant rate of the circumferential strain equal to 0.002 mm/s has permitted to completely detect the load–displacement curve, even in case of severe snap-back. Such a device is particularly effective in controlling the post-peak phase for specimens with slenderness values lower than 3.0, and characterized by a splitting failure mode. However, when the sample slenderness is larger than 3.0, the failure does not always occur at the middle of the specimen and, therefore, the circumferential expansion at mid-height is no longer a stable parameter during the loading process. In these cases, an alternative method of feedback control can be based on the inelastic part of the total deformation [3].

Also in this case, during the tests each specimen was monitored by means of AE. The AE hits emerging from the compressed specimens were detected by applying to the sample surface a piezoelectric (PZT) transducer, sensitive in the same frequency range of that applied on the specimens controlled by the axial displacement.

The load vs. axial displacement diagrams for the considered specimens are reported in Figs. 10 and 12, showing both global and local snap-back instabilities evidenced by the positive slope in the softening branch.

As regards the crushing energies, they are $G_C \sim 19$ N/mm for the gypsum specimen with $\lambda = 1.0$, and $G_C \sim 1.4$ N/mm for the gypsum specimen with $\lambda = 2.0$. The corresponding values of the total dissipated energy, D, are: 95 J ($\lambda = 1.0$) and 7 J ($\lambda = 2.0$), respectively.

Concerning the stability of the compression loading process, by the application of Eq. (1), it is verified that, for the gypsum specimen with $\lambda = 1.0$, $B = 1.37$ (stable post-peak regime), whereas for the gypsum specimen with $\lambda = 2.0$, $B = 0.39$ (unstable post-peak regime).

As regards the specimen with slenderness $\lambda = 2.0$, the cumulative number of AE events is represented in Fig. 11, together with the load vs time diagram. In spite of the loading drops (snap-back instabilities) in the post-peak regime, no AE bursts (emitted energy, E) are observed in the cumulated curve, due to the fact that the loading process is controlled by a monotonically increasing function of time, and the snap-back instability is captured experimentally. Therefore, the dissipated energy, D, computed above, is equal to the total released energy, R, because no emitted energy, E, is detected (R = D).

Also for the specimen with slenderness $\lambda = 1.0$ (Fig. 13), no burst is detected in the AE cumulated curve, in spite of the local negative jumps in the softening branch of the load vs. time diagram, the snap-back instabilities being captured experimentally. Also

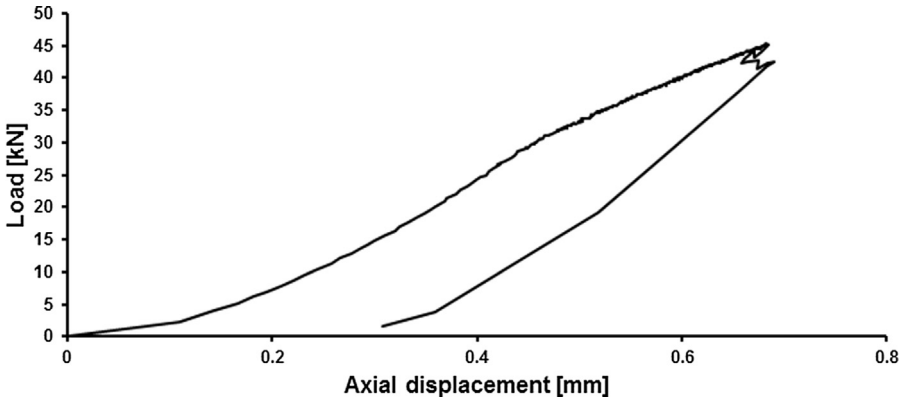

Fig. 10. Load vs. axial displacement for a gypsum specimen of slenderness 2 subjected to a compression test. Local and global snap-back instabilities emerge in the post-peak branch.

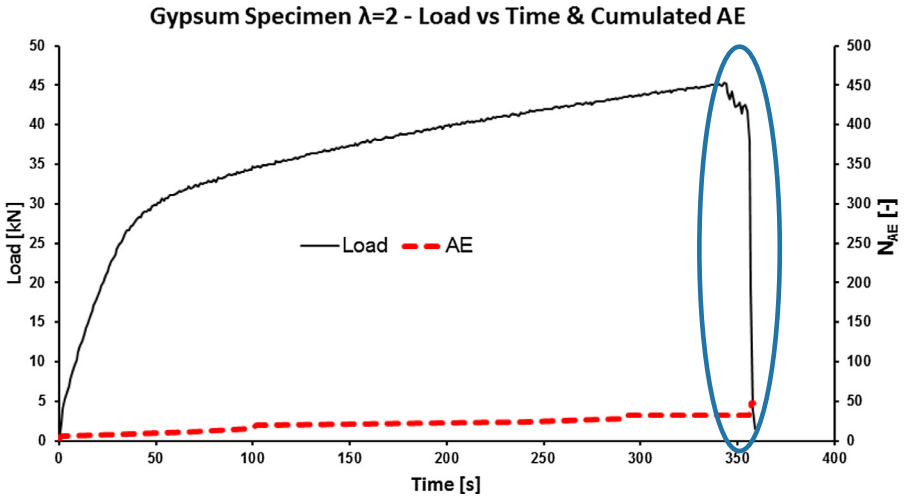

Fig. 11. Load vs. time diagram and AE cumulated curve for a gypsum specimen of slenderness 2 subjected to a compression test controlled by the circumferential elongation. In spite of the loading drops (snap-back instabilities) in the post-peak regime, no AE bursts (emitted energy, E) are observed in the cumulated curve, due to the adopted circumferential strain control.

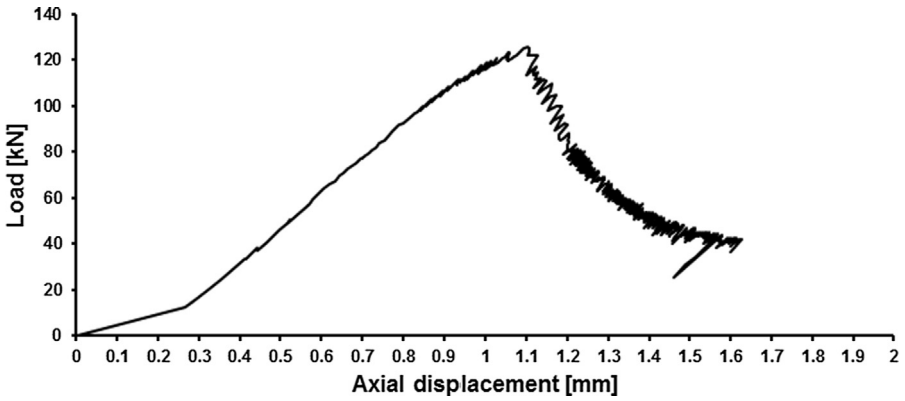

Fig. 12. Load vs. axial displacement for a gypsum specimen of slenderness 1 subjected to a compression test. A series of slight and multiple loading drops (local snap-back instabilities) emerges in the post-peak branch.

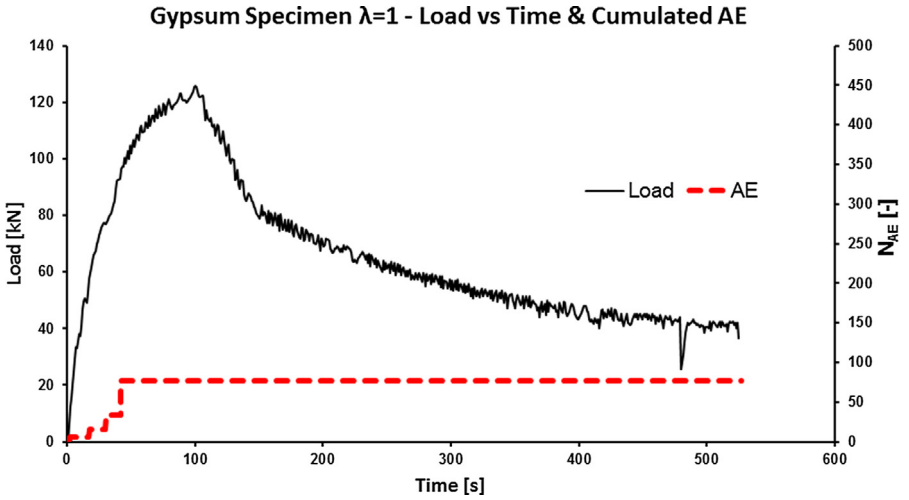

Fig. 13. Load vs. time diagram and AE cumulated curve for a gypsum specimen of slenderness 1 subjected to a compression test controlled by the circumferential elongation. In spite of the slight loading drops (snap-back instabilities) in the softening branch, no AE bursts (emitted energy, E) is observed in the cumulated curve.

in this case, the dissipated energy is equal to the total released energy (R = D).

7. Conclusions

In this paper the results of experimental tests carried out on cylindrical samples of gypsum are analyzed, in order to demonstrate that the energy emitted during the loading process is generally due to snap-back instabilities. Gypsum samples with different slenderness are considered, and all the tests are monitored by using the Acoustic Emission (AE) technique.

In particular, the cumulative number of AE signals is used to calculate the emitted energy, E, which is equal to the difference between the energy released during the loading, R, and the dissipated energy, D (R = D + E).

For the analyzed samples showing a brittle behavior, the crack propagation occurs suddenly with a catastrophic drop in the load carrying capacity, and the resulting emitted energy appears with a burst in the AE cumulative curve. On the other hand, to get the complete load vs. displacement response, other tests were controlled by the circumferential elongation, measured with a circumferential chain positioned around the half-height of the specimen. In the brittle cases, both load and displacement must decrease in order to obtain a controlled crack propagation, and consequently no AE hits due to snap-back phenomena are observed, because the energy is totally dissipated in order to create new fracture surfaces. It proves that crushing or fracture energy and AE energy are independent physical quantities, the latter resulting from local instabilities in the structural response.

References

[1] Bocca P, Carpinteri A. Snap-back fracture instability in rock specimens: experimental detection through a negative impulse. Engng Fract Mech 1990;35:241–50.
[2] Carpinteri A. Notch sensitivity in fracture testing of aggregative materials. Engng Fract Mech 1982;16:467–81.
[3] Carpinteri A, Corrado M, Lacidogna G. Heterogeneous materials in compression: correlations between absorbed, released and acoustic emission energies. Engng Fail Anal 2013;33:236–50.
[4] Carpinteri A, Lacidogna G, Pugno N. Structural damage diagnosis and life-time assessment by acoustic emission monitoring. Engng Fract Mech 2007;74:273–89.
[5] Carpinteri A. Size effects on strength, toughness, and ductility. J Engng Mech 1989;115:1375–92.
[6] Carpinteri A, Accornero F. Multiple snap-back instabilities in progressive microcracking coalescence. Engng Fract Mech 2018;187:272–81.
[7] Carpinteri A. Post-peak and post-bifurcation analysis of cohesive crack propagation. Engng Fract Mech 1989;32:265–78.
[8] Carpinteri A, Colombo G. Numerical analysis of catastrophic softening behaviour (snap-back instability). Comput Struct 1989;31:607–36.
[9] Carpinteri A. Cusp catastrophe interpretation of fracture instability. J Mech Phys Solids 1989;37:567–82.
[10] Aggelis DG. Classification of cracking mode in concrete by acoustic emission parameters. Mech Res Commun 2011;38:153–7.
[11] Carpinteri A, Lacidogna G, Accornero F, Mpalaskas A, Matikas T, Aggelis D. Influence of damage on the acoustic emission parameters. Cem Concr Compos 2013;44:9–16.
[12] Carpinteri A, Lacidogna G, Invernizzi S, Accornero F. The sacred mountain of Varallo in Italy: seismic risk assessment by Acoustic Emission and structural numerical models. Sci World J 2013:1–10.
[13] Lacidogna G, Accornero F, Corrado M, Carpinteri A. Crushing and fracture energies in concrete specimens monitored by Acoustic Emission. Proceedings of the 8th international conference on fracture mechanics of concrete and concrete structures, FraMCoS; 2013. p. 1726–36.
[14] Accornero F, Invernizzi S, Lacidogna G, Carpinteri A. Acoustic emission and damage analysis of decorated surface structural supports. 19th European conference on fracture: fracture mechanics for durability, reliability and safety. ECF 2012; 2012.
[15] Lacidogna G, Accornero F, Carpinteri A. Masonry structures. In: Ohtsu M, editor. Innovative AE and NDT techniques for on-site measurement of concrete and masonry structures (RILEM), Chapter 3, Heidelberg: Springer; 2016. p. 27–46.
[16] Grosse CU, Ohtsu M. Acoustic emission testing. Heidelberg: Springer; 2008.
[17] Lockner DA. The role of acoustic emission in the study of rock fracture. Int J Rock Mech Min Sci Geomech 1993;30:883–99.
[18] Mogi K. Magnitude-frequency relationship for elastic shocks accompanying fractures of various materials and some related problems in earthquakes. Bull Earthq Res Inst, University of Tokyo 1962;40:831–53.

[19] Niccolini G, Borla O, Accornero F, Lacidogna G, Carpinteri A. Scaling in damage by electrical resistance measurements. Rendiconti Lincei – Scienze Fisiche Naturali 2014;26:203–9.
[20] Ohtsu M. Recommendation of RILEM TC 212-ACD: acoustic emission and related NDE techniques for crack detection and damage evaluation in concrete: test method for classification of active cracks in concrete structures by acoustic emission. Mater Struct 2010;43:1177–81.
[21] Botvina LR. Damage evolution on different scale levels. Phys Solid Earth 2011;47:859–72.
[22] Godin N, Reynaud P, R'Mili M, Fantozzi G. Identification of a critical time with acoustic emission monitoring during static fatigue tests on ceramic matrix composites: towards lifetime prediction. Appl Sci 2016;6(2):43.
[23] Scholz CH. The frequency-magnitude relation of microfracturing in rock and its relation to earthquakes. Bull. Seismol. Soc. Am. 1968;58:399–415.
[24] Carpinteri A, Lacidogna G, Niccolini G, Puzzi S. Critical defect size distributions in concrete structures detected by the acoustic emission technique. Meccanica 2008;43:349–63.
[25] Carpinteri A, Lacidogna G, Corrado M, Di Battista E. Cracking and crackling in concrete-like materials: a dynamic energy balance. Engng Fract Mech 2016;155:130–44.
[26] Carpinteri A, Corrado M, Paggi M, Mancini G. The overlapping crack model for uniaxial and eccentric concrete compression tests. Mag. Concr Res 2009;61:745–57.
[27] Marolt Čebašek T, Frühwirt T. Investigation of creep behaviours of gypsum specimens with flaws under different uniaxial loads. J Rock Mech Geotech Engng 2018;10:151–63.
[28] Morgan SP, Johnson CA, Einstein HH. Cracking processes in barre granite: fracture process zones and crack coalescence. Int J Fract 2013;180:177–204.
[29] Carpinteri A, Lacidogna G, Accornero F. Evolution of fracturing process in masonry arches. J Struct Eng ASCE 2015;141:1–10.
[30] Accornero F, Lacidogna G, Carpinteri A. Evolutionary fracture analysis of masonry arches: effects of shallowness ratio and size scale. Comptes Rendus Mécanique 2016;344:623–30.
[31] Accornero F, Lacidogna G, Carpinteri A. Medieval arch bridges in the Lanzo Valleys, Italy: incremental structural analysis and fracturing benefit. J Bridge Eng ASCE 2018. http://dx.doi.org/10.1061/(ASCE)BE.1943-5592.0001252.
[32] Lockner D. The role of acoustic emission in the study of rock fracture. Int J Rock Mech Min Sci Geomech Abstr 1993;30(7):883–99.
[33] Rao MVMS, Prasanna Lakshmi KJ. Analysis of *b*-value and improved *b*-value of acoustic emissions accompanying rock fracture. Curr Sci 2005;89(9):1577–82.
[34] Chang SH, Lee CI. Estimation of cracking and damage mechanisms in rock under triaxial compression by moment tensor analysis of acoustic emission. Int J Rock Mech Min Sci 2004;41(7):1069–86.
[35] Lacidogna G, Manuello A, Niccolini G, Accornero F, Carpinteri A. Acoustic emission wireless monitoring of structures. In: Ohtsu M, editor. Acoustic emission and related non-destructive evaluation techniques in the fracture mechanics of concrete, Chapter 2. Cambridge: Woodhead Publishing; 2015. p. 15–40.
[36] Carpinteri A, Corrado M, Lacidogna G. Three different approaches for damage domain characterization in disordered materials: fractal energy density, *b*-value statistics, renormalization group theory. Mech Mater 2012;53:15–28.